

Honeycomb Wachspress finite elements for structural topology optimization

Cameron Talischi · Glaucio H. Paulino · Chau H. Le

Received: 19 November 2007 / Revised: 7 February 2008 / Accepted: 9 March 2008 / Published online: 22 May 2008
© Springer-Verlag 2008

Abstract Traditionally, standard Lagrangian-type finite elements, such as linear quads and triangles, have been the elements of choice in the field of topology optimization. However, finite element meshes with these conventional elements exhibit the well-known “checkerboard” pathology in the iterative solution of topology optimization problems. A feasible alternative to eliminate such long-standing problem consists of using hexagonal (honeycomb) elements with Wachspress-type shape functions. The features of the hexagonal mesh include two-node connections (i.e. two elements are either not connected or connected by two nodes), and three edge-based symmetry lines per element. In contrast, quads can display one-node connections, which can lead to checkerboard; and only have two edge-based symmetry lines. In addition, Wachspress rational shape functions satisfy the partition of unity condition and lead to conforming finite element approximations. We explore the Wachspress-type hexagonal elements and present their implementation using three approaches for topology optimization: element-based, continuous approximation of material distribution, and minimum length-scale through projection functions. Examples are presented that demonstrate the advantages of the proposed element in achieving checkerboard-free solutions and avoiding spurious fine-scale patterns from the design optimization process.

Keywords Topology optimization · Checkerboard · Wachspress interpolation functions · Continuous approximation of material distribution · Projection functions

1 Nomenclature

$c(\rho, \mathbf{u})$	Compliance of the design
c_i	Normalizing shape function coefficient
p	SIMP penalty exponent
$q(\mathbf{x})$	Curve encompassing the points of intersection of edges
r_j	Distance from the quadrature points to the origin
r_{\min}	Radius of projection
w_j	Weight for the group of quadrature points
C_{ijkl}	Components of the elastic stiffness tensor
C_{ijkl}^H	Components of the homogenized stiffness tensor
E^0	Stiffness of solid phase
N_i	Shape function corresponding to node i
S_i	Set of elements sharing node i
V_h	Set of all Y-periodic functions
V_s	Specified volume fraction
Y	Periodic domain
α_j	Angle corresponding to the quadrature group
$\lambda_i(\mathbf{x})$	Straight line going through nodes i and $i + 1$
ρ_e	Density of element e
ρ_i^e	Nodal density corresponding to node i of element e
χ_p^{kl}	Characteristic displacements
ρ_{\min}	Density lower bound
Ω	Extended design domain
Ω_e	Regular hexagonal domain

C. Talischi · G. H. Paulino (✉) · C. H. Le
Department of Civil and Environmental Engineering,
University of Illinois at Urbana-Champaign,
Newmark Laboratory, 205 North Mathews Avenue,
Urbana, IL 61801, USA
e-mail: paulino@uiuc.edu

Ω_s	Material subset of the extended design domain
\mathbf{f}	Global load vector
$\mathbf{f}^{(kl)}$	Material load corresponding to test strain kl
\mathbf{x}_i	Coordinates of node i
\mathbf{u}	Global displacement vector
$\boldsymbol{\varepsilon}^{0(kl)}$	Test strain
\mathbf{B}	Strain-displacement matrix
\mathbf{C}^0	Constitutive matrix of the solid phase
\mathbf{C}_e	Constitutive matrix for element e
\mathbf{K}	Global stiffness matrix
\mathbf{K}_e	Element stiffness matrix
\mathbf{K}_e^0	Stiffness matrix for solid reference element

2 Introduction

Topology optimization methods seek to find the optimal layout or topology of a fixed amount of material that satisfies a required set of design demands. With significant advancements in the recent years and application to a wide range of practical problems, topology optimization has emerged as a powerful and robust tool for the design of structural, mechanical, and material systems. Despite the maturity of the field, however, there remains a class of numerical issues such as the well-known checkerboard problem that continues to be the focus of extensive research. This paper introduces a new element for the implementation of topology optimization and demonstrates its effectiveness in removing the checkerboard pathology.

Traditionally, the topology design is formulated as a material distribution problem, in which every point of the candidate design domain represents either a material or a void region. However, the optimal material distribution problem as such is ill-posed, lacking solutions in the continuum setting (Murat and Tartar 1985; Kohn and Strang 1986; Sigmund and Petersson 1998). The existence of solutions may be achieved through a relaxation of the solid/void formulation. For example, the homogenization method, introduced by Bendsøe and Kikuchi (1988), extends the space of admissible designs to include solutions with microstructural features, whose homogenized properties are used to determine the mechanical behavior of the design. Likewise, the Solid Isotropic Material with Penalization (SIMP) model relaxes the original “0–1” problem by considering a continuous material “density” as the design variable and a power-law relation for interpolating the material properties of the intermediate densities (Bendsøe 1989; Zhou and Rozvany 1991). This inter-

polation also serves as a penalization that steers the optimization procedure toward a final design without intermediate densities. For a discussion on the relationship between the two methods and the physical interpretation of the SIMP model refer to Bendsøe and Sigmund (1999). Unfortunately, the topology optimization solutions with both methodologies suffer from the checkerboard phenomenon, where the optimized designs may contain patches of alternating material and void elements.

The checkerboard solutions appear as a result of inadequate or poor numerical modeling. Diaz and Sigmund (1995) attributed the formation of checkerboard as a local instability to the error in the finite element approximation. The checkerboard pattern has an artificially high stiffness when modeled by lower order finite elements so it is economical in the optimization process. In a related investigation, Jog and Haber (1996) addressed general numerical instabilities in topology optimization by formulating the corresponding mixed variational problem and concluded that insufficient interpolation of the displacement field can lead to unstable modes. Again, it was confirmed that the degree of approximation and choice of finite elements plays a crucial role in the appearance of numerical anomalies such as checkerboard. Therefore, it is expected that more accurate modeling of the mechanical behavior of the design would alleviate the checkerboard problem. In fact, higher-order discretizations using quadratic displacement elements have been shown to be more stable even though the final designs may exhibit mild forms of checkerboard, depending on the severity of the penalization (Diaz and Sigmund 1995). Non-conforming elements can also give checkerboard-free solutions since they correctly capture the vanishing stiffness of checkerboard (Jang et al. 2003, 2005). The drawback of using non-conforming shape functions is that they do not preserve the continuity of the field across elements; they allow negative field approximation and may suffer from other numerical issues (e.g. lack of convergence).

The abovementioned studies were primarily concerned with the effects of finite element modeling on the stability of topology optimization in the context of element-based formulation, in which the design variable is the uniform density assigned to each displacement element. It turns out that this discontinuous representation of the material field is conducive to the appearance of checkerboard. Considering the representation of the design field, a handful of methods of checkerboard suppression introduce explicit restrictions on the local variation of the material density so

that the undesirable material layouts like checkerboard are avoided. Poulsen (2002a) used a descriptor function to identify corner contacts throughout the design domain at each iteration step and added a constraint to prohibit their formation. Expanding on this idea, Pomezanski et al. (2005) explored other possible “corner contact” functions that could also eliminate the grey checkerboards. To achieve geometric control over the formation of checkerboard, Wavelet methods have also been applied to topology optimization (Poulsen 2002b; Yoon and Kim 2005). Sigmund and Petersson (1998) discussed the addition of slope constraints to control the density gradient and concluded that this approach can establish a well-behaved topology optimization procedure by arbitrarily weakening the numerical instabilities.

Other methods have been proposed that constrain the gradient of material field implicitly by using nodal densities as the design variables. In one approach (Matsui and Terada 2004; Rahmatalla and Swan 2004), the continuity of the material field is enforced by using finite element shape functions to interpolate the density throughout the design domain from nodal densities. As a result of this choice of density field representation, the discontinuous checkerboard patches are naturally excluded from the design space. However, other forms of numerical instabilities such as “islanding” and “layering” effects have been observed with these formulations (Rahmatalla and Swan 2004). Alternatively, Guest et al. (2004) used a projection function with an embedded length scale to extract element densities from nodal densities. This method has the added effect of establishing a minimum member size and generating mesh-independent solutions. The problem of mesh-dependency, linked to the ill-posedness of the continuum problem, arises when the optimal designs have finer members as more refined meshes are used. Since the checkerboard is a fine-scaled feature, it may be removed if a proper length scale is imposed on the optimization. Other methods that address the mesh-dependency problem include the perimeter control (Ambrosio and Buttazzo 1993; Haber et al. 1996), density and sensitivity filters (Bruns 2005; Wang and Wang 2005), monotonicity-based method (Poulsen 2003), regularized density control (Borrvall and Petersson 2001b), and more recently the morphology-based techniques (Sigmund 2007). Although these methods have the desirable effects of generating mesh-independent solutions and in some cases improved convergence, there remains interest in obtaining checkerboard-free solutions without imposing any further constraints. The topology designs based

on these approaches may be very sensitive to the choice of parameters (e.g. filter characteristics) and can potentially augment the physical model and the optimization process.

It is evident from the above discussion that the approximation of the two distinct fields of displacement and density greatly influences the stability of the topology optimization problem. In this work, we address the checkerboard issue by introducing the Wachspress hexagonal element which possesses desirable characteristics in representing both fields: the hexagonal mesh prohibits one-node connections and subsequently checkerboard patterns, while the interpolation functions of the Wachspress element eliminate the appearance of spurious fine-scale patterns from the design optimization. Thus, checkerboard-free solutions are obtained without any further restrictions or filtering.

Topology optimization with honeycomb meshes has also been explored by Saxena and Saxena (2007) and Langelaar (2007). For two-dimensional problems, the discretization is constructed using lower order finite elements in both cases: Saxena and Saxena (2007) split each hexagon into two quads while Langelaar (2007) uses the union of six triangles to achieve the desired discretization. We note that the choice of dividing the hexagonal elements in such an approach is not unique. For instance, the hexagonal cells can be either split vertically, or along the left or right diagonal and this introduces ambiguity in the finite element discretization (see Fig. 3 of Saxena and Saxena 2007). Moreover, this approach is limited to constant element density formulations since T3/T3 and Q4/Q4 elements suffer from islanding/layering instabilities. Our proposed approach of using Wachspress shape functions circumvents such issues and can be readily extended for continuous density representations as it defines an actual finite element (see Section 4). The use of Wachspress shape functions was first presented in the Multiscale and Functionally Graded Materials (M&FGM 2006) Conference (Talischi et al. 2008).

The remainder of the paper is organized as follows: in the next two sections, we discuss the geometric properties of the new element (Section 3) and the construction of Wachspress shape functions (Section 4). In Section 5, we present the numerical integration scheme for the new element. Next we outline the topology optimization formulation for the compliance minimization problem with different material field representations. In Section 7, we address the stability of the hexagonal Wachspress element by investigating its susceptibility to fine-scale patterns. We show numerical results for

the new implementation in Section 8 to confirm its robustness. Finally, we conclude the paper with some remarks in Section 9.

3 Hexagonal elements and the role of meshing

Before discussing the construction and properties of the Wachspres hexagonal element, it is constructive to make a few remarks regarding the role of meshing in topology optimization. First we note that even though it is possible to use a non-uniform mesh, it is customary to model topology optimization problems with uniform meshes. When employing non-uniform meshes, great care must be taken to avoid favoring any part of the design domain because, *a priori*, one does not know where the final solution will lie. For example, in adaptive schemes where one attempts to obtain high resolution solutions inexpensively, the criteria for adaptive refinement or de-refinement of the mesh becomes a critical issue in correctly capturing the optimal solution (Maute and Ramm 1995; Costa and Alves 2003; Wang 2007). Moreover, the greatest portion of the computational cost in some topology optimization problems, such as compliance minimization, is due to solving the equilibrium equations and a uniform mesh eliminates the need for repeated computation of various local stiffness matrices (Borrvall and Petersson 2001a).

If we restrict ourselves to uniform meshes, there are only three possible regular tessellations in two dimensions, namely those generated by equilateral triangles, squares, and hexagons (see, for example, Chavey 1989). Since the first two have been widely utilized in topology optimization, it is reasonable to explore the other possibility as a feasible alternative. In fact, we recognize that the hexagonal tessellation is distinguished from the other two in that it does not allow for corner contacts. That is, two connected hexagonal tiles must share an edge and have two common vertices (see Fig. 1). Consequently, unlike triangular and quadrilateral grids, the

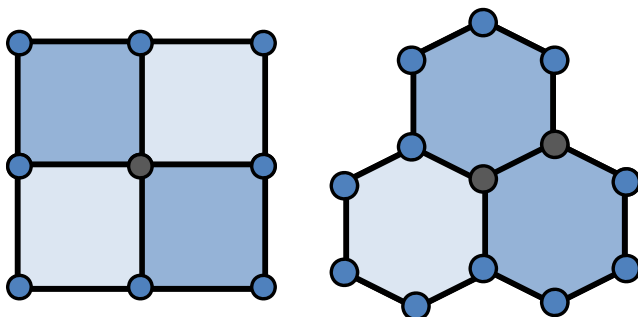


Fig. 1 Quadrilateral meshes can display one-node connections, while in a hexagonal mesh two connected elements always share two nodes through an edge connection

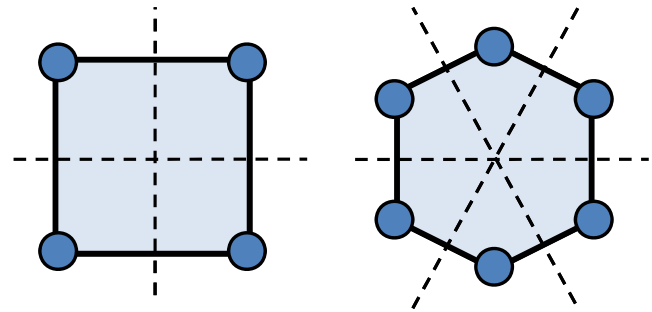


Fig. 2 The Q4 element has two edge-based symmetry lines, while the hexagonal element has three edge-based symmetry lines

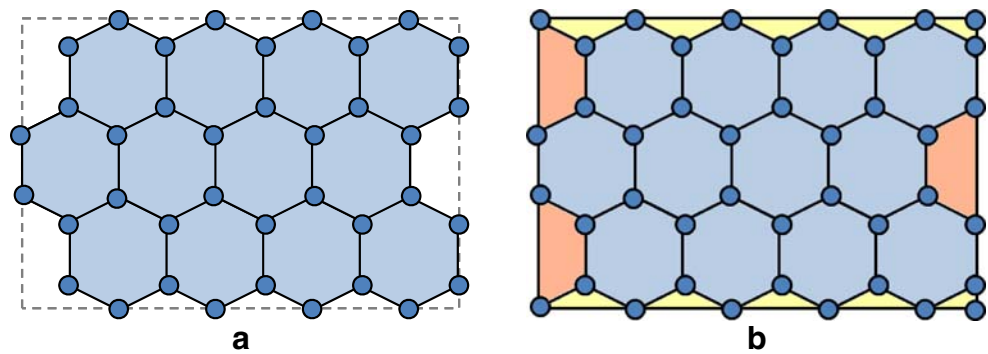
hexagonal tessellation, by the virtue of its geometry, constrains the material layout and naturally excludes the unwanted formation of checkerboard and one-node hinges. Note that higher-order triangular and quadrilateral elements may suffer from one-node hinges even though the more accurate approximation of the displacement field may mitigate the checkerboard problem. Employing hexagonal meshes, on the other hand, simply eliminates the possibility of checkerboard and one-node hinge formations without the need for imposing any further restrictions. Another appealing feature of the hexagonal element is that it has more lines of symmetry per element compared to the triangular and square elements and, consequently, suffers from less directional constraint and allows for a more flexible arrangement of the final layout in the optimization process (Fig. 2).

We must point out that in order to model a domain with straight boundaries using a hexagonal mesh, it is necessary to insert one layer of triangular and quadrilateral elements along the boundary (see Fig. 3). Linear triangular (T3) and bilinear quadrilateral elements (Q4) are used in this study. The difference in element size must be considered when enforcing the volume constraint, and the related parameters must be adjusted accordingly. Since only one layer of these elements is needed to straighten the boundary, their effect on the optimization procedure is expected to be negligible. In fact our numerical experiments show that the optimal solutions remain qualitatively unchanged when these elements are placed around the boundary.

4 Wachspres shape functions

In this work, we adopt Wachspres rational interpolation functions for the proposed hexagonal element. Wachspres introduced general interpolants for convex polygons, and his pioneering work provided a basis for further development of polygonal finite element formulations (Wachspres 1975). Wachspres interpolants

Fig. 3 Domain discretization with Wachspress hexagonal mesh: **a** domain without “boundary” elements **b** domain with “boundary” elements (standard quads and triangles)



were developed using concepts of projective geometry and are the lowest order functions that satisfy the conditions of boundedness, linear precision, and global continuity (Warren 2003; Sukumar and Malsch 2005). Although the Wachspress method can be extended to obtain higher order shape functions, the element examined in this work is a first-order element.

For an n -sided polygon, the Wachspress shape functions N_i for $i = 1, \dots, n$ are given by the ratio of two polynomials, with degree $(n - 2)$ for the numerator, and $(n - 3)$ for the denominator (e.g. Dasgupta 2003):

$$N_i(x_1, x_2) = \frac{P_{n-2}(x_1, x_2)}{P_{n-3}(x_1, x_2)} \tag{1}$$

In the following paragraphs, we discuss a geometric construction of these shape functions based on the algebraic equations of the edges of the polygonal domain. Alternatively, it is possible to compute the coefficients of the numerator and the denominator of Wachspress functions symbolically (Dasgupta 2003) or numerically (Dalton 1985).

Let Ω_e denote the regular hexagonal domain (see Fig. 4). The shape function N_i , corresponding to node i , is given by:

$$N_i(\mathbf{x}) = c_i \frac{\lambda_{i+2}(\mathbf{x}) \lambda_{i+3}(\mathbf{x}) \lambda_{i+4}(\mathbf{x}) \lambda_{i+5}(\mathbf{x})}{q(\mathbf{x})} \tag{2}$$

where $\lambda_{i+1}(\mathbf{x}) = 0$ represents the straight line going through nodes “ i ” and “ $i + 1$ ” while $q(\mathbf{x}) = 0$ is the equation of the circle encompassing the points of intersection of the extensions of the edges. It is understood that $\lambda_7 = \lambda_1$, $\lambda_8 = \lambda_2$ and so on. In other words, the numerator is the product of the equations of the edges not intersecting the given node. The c_i coefficient is a normalizing factor, which is given by:

$$c_i = \frac{q(\mathbf{x}_i)}{\lambda_{i+2}(\mathbf{x}_i) \lambda_{i+3}(\mathbf{x}_i) \lambda_{i+4}(\mathbf{x}_i) \lambda_{i+5}(\mathbf{x}_i)} \tag{3}$$

Here \mathbf{x}_i represents the nodal coordinates. A typical conforming shape function is shown in Fig. 5.

Wachspress rational shape functions satisfy the necessary conditions for conforming Galerkin approximations (Sukumar and Tabarraei 2004; Sukumar and Malsch 2005). First, these shape functions are bounded, non-negative and form a partition of unity:

$$\sum_{i=1}^6 N_i(\mathbf{x}) = 1, \quad 0 \leq N_i(\mathbf{x}) \leq 1 \tag{4}$$

Since the Wachspress shape functions are non-negative, they can be used to interpolate the density field (see discussion on CAMD in Section 6). This is not possible with higher order (e.g. Q8 and Q9 quads) or non-conforming elements. Furthermore, they exhibit the Kronecker-delta property which simplifies applying the necessary boundary conditions:

$$N_i(\mathbf{x}_j) = \delta_{ij} = \begin{cases} 0, & i \neq j \\ 1, & i = j \end{cases} \tag{5}$$

Also, these shape functions can reproduce a linear function (exhibit linear precision), and thus satisfy the

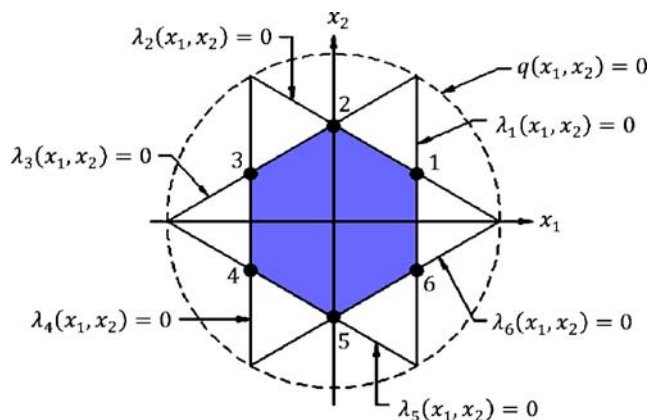


Fig. 4 Hexagonal element domain illustrated for the construction of Wachspress shape functions

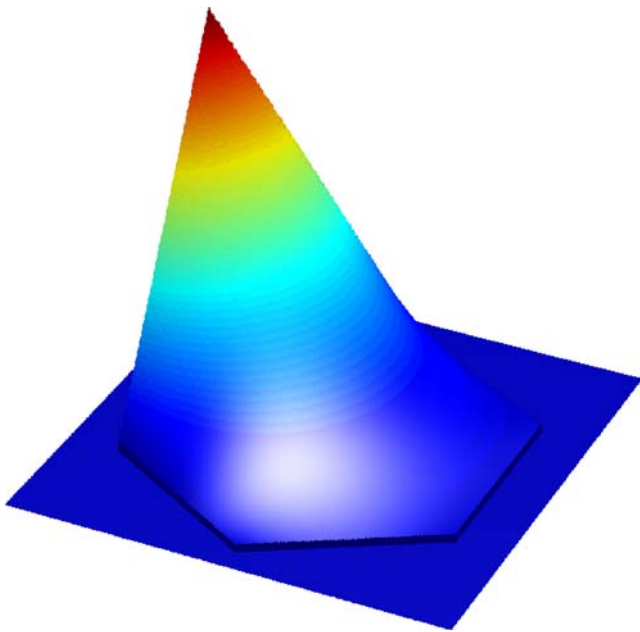


Fig. 5 Typical Wachspress shape function (the value of the shape function is raised on the edges for better visualization)

sufficient condition of convergence for second-order partial differential equations:

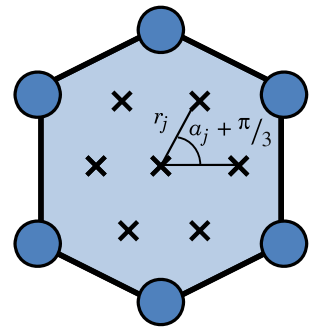
$$\sum_{i=1}^6 N_i(\mathbf{x}) \mathbf{x}_i = \mathbf{x} \quad (6)$$

Finally, the Wachspress shape functions provide C^0 continuous field approximations over the domain, and thus lead to a conforming representation. The element performance in solving second-order boundary-value elliptical problems has been studied by Gout (1985), who compared this element with polynomial finite elements of the same degree.

5 Numerical integration for hexagonal elements

For uniform meshes, the constant element density implementation using the SIMP model requires the computation of the stiffness matrix only once, while the CAMD approach (see the following section for more details) requires that the element stiffness matrices be evaluated at each iteration step. Therefore the efficiency of the integration method must be considered in choosing the appropriate scheme. One possibility is to partition the element into triangular regions and apply the commonly used quadrature rules on each triangle (Sukumar and Tabarraei 2004). An alternative is to use the quadrature rules developed for polygonal domains, specifically the fully symmetric quadrature for regions with regular hexagonal symmetry given by Lyness and Monegato (1977). We have adopted the

Fig. 6 Schematic illustration of the quadrature rule for the regular hexagonal element: integration points are shown with “x” marks



second approach since it is more practical and uses the least number of quadrature points for a given degree of accuracy.

The method is illustrated in Fig. 6. The quadrature rule is invariant under 60° rotation due to the hexagonal symmetry of the integration region, and may be expressed in the following form:

$$\int_{\Omega_e} f d\Omega \approx w_0 f(0, 0) + \sum_{j=1}^N \sum_{i=1}^6 w_j f\left(r_j, \alpha_j + \frac{\pi i}{3}\right) \quad (7)$$

Here w_j represents the weight corresponding to the quadrature point at distance r_j from the origin and angle $\alpha_j + \frac{\pi i}{3}$ from the horizontal axis for each $1 \leq i \leq 6$. The list of quadrature points for various values of j can be found in the original reference (Lyness and Monegato 1977), and for completeness, are provided in Table 1 of the Appendix. In our implementation, we used $N = 1$ (i.e. 7 quadrature points including the origin) which corresponds to degree 5 polynomial accuracy.

6 Topology optimization formulation

The performance of the proposed hexagonal element is assessed through the implementation of benchmark compliance minimization problems. In this class of problems, the objective is to find the least compliant (i.e. stiffest) layout of a fixed volume of material within a pre-defined design domain, subjected to given traction and displacement boundary conditions. As mentioned before, the topology or layout of the structure is commonly described by material “density” design variables. By convention, density value of one at any point in the design domain signifies a material region while the voids are represented by zero density. Subsequently, the designed structure Ω_s is defined as the material subset of the design domain Ω :

$$\rho(\mathbf{x}) = \begin{cases} 0, & \mathbf{x} \notin \Omega_s \\ 1, & \mathbf{x} \in \Omega_s \end{cases} \quad (8)$$

As mentioned before, the problem is relaxed to allow for continuous variation of density in $[\rho_{min}, 1]$. Placing the positive lower bound ρ_{min} helps prevent the singularities of the global stiffness matrix. In this work, we use SIMP as the material model which gives the following power-law relation to define the stiffness of intermediate densities:

$$E(\mathbf{x}) = \rho(\mathbf{x})^p E^0, \quad p > 1$$

$$\rho_{min} \leq \rho(\mathbf{x}) \leq 1 \tag{9}$$

where E^0 denotes the stiffness of the solid phase. With value of p greater than 1, the stiffness of the intermediate densities becomes small compared to their contribution to total volume of the structure, making them unfavorable in the optimization process. Therefore, this penalization steers the optimization process to a 0–1 design.

Using this density parameter as the design variable, the minimum compliance problem in the discrete form is formulated as (see, for example, Bendsøe and Sigmund 2003):

$$\min_{\rho, \mathbf{u}} \quad c(\rho, \mathbf{u}) = \mathbf{f}^T \mathbf{u}$$

$$\text{s.t.} \quad \mathbf{K}(\rho) \mathbf{u} = \mathbf{f}$$

$$\int_{\Omega} \rho dV = V_s \tag{10}$$

Here $c(\rho, \mathbf{u})$ is the objective function (i.e. the compliance of the structure) and \mathbf{f} and \mathbf{u} are the global force and displacement vectors. Moreover, \mathbf{K} represents the global stiffness matrix, which is dependent on the density distribution. The parameter V_s is the specified maximum volume of structural material.

In order to solve this optimization problem, we must choose a proper discretization of the design field. We consider the following three different approaches for implementation of the Wachspress hexagonal element:

1. Element-based
2. Continuous Approximation of Material Distribution (CAMD)
3. Projection Method to achieve minimum length scale

Although these approaches do not exhaust the possible discretizations of the density field, we have limited our investigation of the Wachspress element to these cases in order to assess its performance against the corresponding numerical problems, namely the checkerboard and islanding/layering instabilities, and mesh-dependency.

6.1 Element-based approach

In the element based approach, a uniform density parameter ρ_e is assigned to each displacement finite

element. The element densities become the design variables, and their sensitivities are calculated using the adjoint method:

$$\frac{\partial c}{\partial \rho_e} = -\mathbf{u}_e^T \frac{\partial \mathbf{K}_e}{\partial \rho_e} \mathbf{u}_e = -p \rho_e^{p-1} \mathbf{u}_e^T \mathbf{K}_e^0 \mathbf{u}_e \tag{11}$$

As discussed previously, the element-based implementation using linear triangular and bilinear quadrilateral displacement elements suffer from the checkerboard.

6.2 Continuous Approximation of Material Distribution (CAMD)

Alternatively, we can define the design parameters to be the nodal densities, from which the density through the domain is interpolated. An appealing feature of this density parameterization is that, irrespective of the interpolation scheme, the local variation of density is restricted. Since adjacent elements share nodal densities, the change from solid to void must occur across at least one element, thus making the checkerboard formation impossible. We consider two possible interpolation schemes. Based on the concept of graded elements (Kim and Paulino 2002; Silva et al. 2007), we use shape functions to obtain the density within each element and throughout the design domain:

$$\rho(\mathbf{x}) = \sum_{e=1}^n \sum_{i=1}^6 N_i^e(\mathbf{x}) \rho_i^e \tag{12}$$

Here ρ_i^e denotes the nodal density of element e , which is taken to be coincident with the corresponding displacement node (Fig. 7). Incidentally, this condition is not necessary and one may explore the cases where the displacement and density meshes are not coincident. This approach for topology optimization is referred to as the Continuous Approximation of Material Distribution

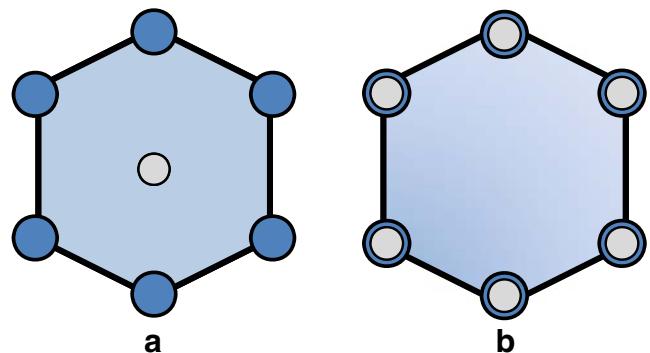


Fig. 7 A schematic illustration of the displacement and density approximation: **a** H6/U element **b** H6/H6 element (CAMD). Larger circle represents displacement nodes, while the smaller circle represents the density design variable

(CAMD; Matsui and Terada 2004). In an investigation by Rahmatalla and Swan (2004) it was discovered that even though the solutions with Q4/Q4 do not exhibit the checkerboard patterns, they may suffer from other numerical instabilities such as “islanding” and “layering.” This observation is also confirmed by Jog and Haber’s (1996) study, in which they determined the Q4/Q4 implementation to be unstable.

The sensitivities of the objective function with respect to the nodal densities in the CAMD implementation can be computed as follows:

$$\frac{\partial c}{\partial \rho_i^e} = - \sum_{e \in S_i} \mathbf{u}_e^T \frac{\partial \mathbf{K}_e}{\partial \rho_i^e} \mathbf{u}_e \tag{13}$$

Here S_i is the set of all elements sharing node i . The element stiffness matrix is given by:

$$\mathbf{K}_e = \int_{\Omega_e} \left(\sum_{j=1}^6 N_j^e \rho_j^e \right)^p \mathbf{B}^T \mathbf{C}^0 \mathbf{B} d\Omega \tag{14}$$

where \mathbf{B} denotes the strain-displacement matrix and \mathbf{C}^0 is the constitutive matrix of the solid phase. Using this relation, we can compute the sensitivity of the stiffness matrix with respect to the nodal densities:

$$\frac{\partial \mathbf{K}_e}{\partial \rho_i^e} = \int_{\Omega_e} p N_i^e \left(\sum_{j=1}^6 N_j^e \rho_j^e \right)^{p-1} \mathbf{B}^T \mathbf{C}^0 \mathbf{B} d\Omega \tag{15}$$

6.3 Projection method

The other scheme explored in this work is the use of projection functions with a fixed length scale. Proposed by Guest et al. (2004) for Q4 discretization, the method also uses nodal densities as design variables, and assigns to each element a uniform density based on a projection of nodal densities surrounding that element. By choosing a fixed physical radius r_{min} independent of the mesh, one can obtain mesh-independent designs with prescribed minimum member size. The element density is given by a weighted average of nodal densities that are within radius r_{min} from the centroid of that element:

$$\rho_e = \frac{\sum_{i \in S_e} w_i \rho_i}{\sum_{i \in S_e} w_i} \tag{16}$$

Here we have implemented linear weight functions (Fig. 8), which are given by:

$$w_i = \frac{r_{min} - r_i}{r_{min}}, \quad r_i \leq r_{min} \tag{17}$$

where r_i is the distance of the node i from the centroid of element e . However, other weight functions can also be explored.

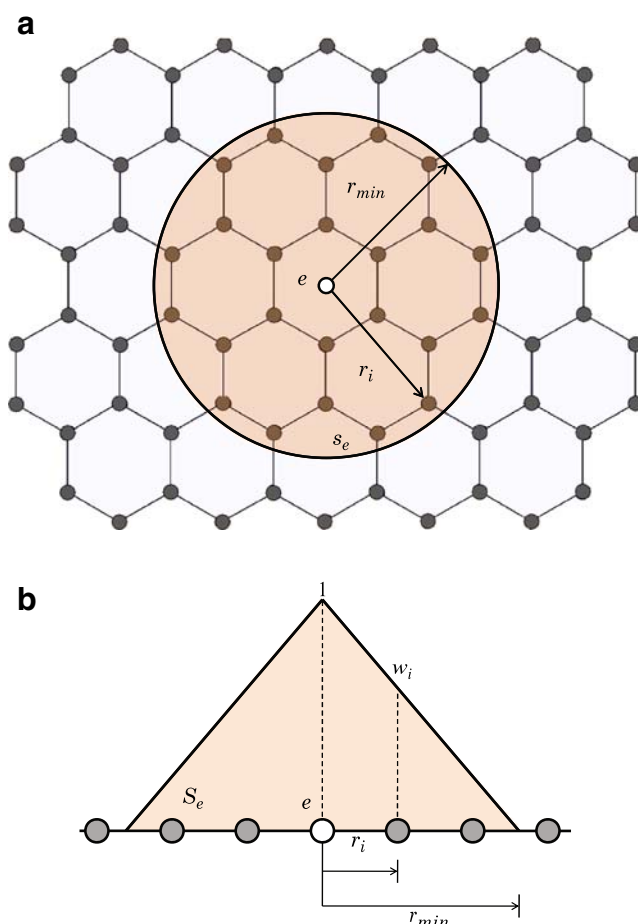


Fig. 8 Projection function: illustration of **a** the domain of influence and **b** the linear weight function

We must point out that it is possible to couple the projection scheme with the CAMD approach by applying the projection function on the nodal densities instead of the element densities. The shape functions can be used to interpolate the density within each element, guaranteeing a prescribed level of smoothness of the density field throughout the domain, while observing the required length-scale. This is especially useful in imposing minimum length scale for topology optimization design of functionally graded structures, where it is necessary to have C^0 continuity of density field to capture the gradation of material properties. Topology optimization of graded structures can be accomplished by means of the FGM-SIMP (Functionally Graded Material–Solid Isotropic Material with Penalization) formulation by Paulino and Silva (2005).

7 Discussion on stability of Wachspress elements

As discussed before, two elements in a hexagonal mesh either share one edge or are not connected at all. Therefore, the geometric nature of the hexagonal Wachspress

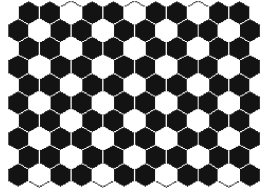
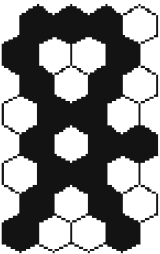
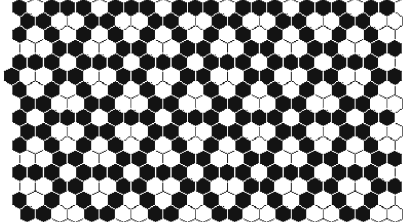
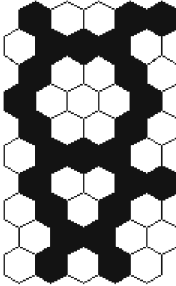
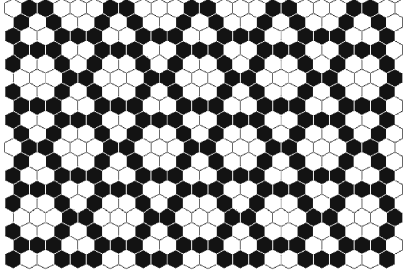
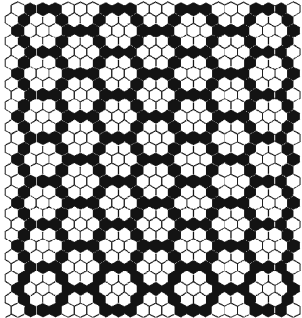
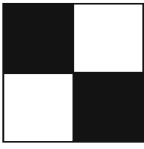
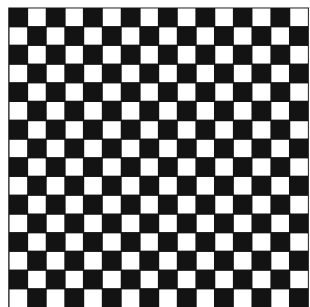
	Unit Cell	Pattern
Pattern 1		
Pattern 2		
Pattern 3		
Pattern 4		
Checkerboard		

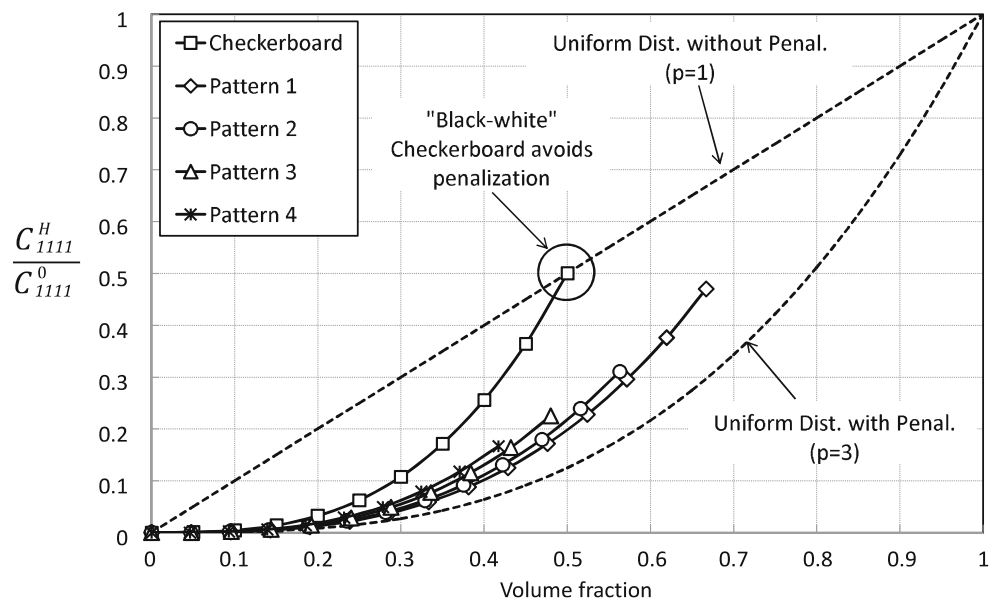
Fig. 9 Small scale patterns of hexagonal elements and their corresponding unit cells

element can eliminate the severe error in the density representation that is observed with the Q4 elements in the form of checkerboard. However, undesired small scale patterns may still be possible with the hexagonal mesh. In this section, we demonstrate that with the proposed formulation, such patterns do not appear as easily as the checkerboard of Q4 elements, establishing the Wachspres element as a more stable element for topology optimization. We accomplish this task by studying the overall stiffness of candidate patterns of hexagonal elements using numerical homogenization. As discussed by Diaz and Sigmund (1995), the appearance of checkerboard in topology stiffness design can be linked to the poor finite element modeling that overestimates its stiffness. As a result of this artificially high stiffness, the checkerboard is stiffer than other arrangements of material and is favored in the optimization process. Following this reasoning, we investigate the susceptibility of topology optimization formulation with Wachspres elements to similar anomalies by considering the behavior of the possible fine scale patterns in the hexagonal mesh (see Fig. 9). In this section, we discuss the numerical procedure for determining the homogenized stiffness of these patterns and compare the results with those obtained for the Q4 element.

The overall stiffness of the patterns may be represented by the homogenized stiffness of repetitive unit cells. According to the theory of numerical homogenization (see, for example, Bendsøe and Sigmund 2003), the homogenized stiffness is calculated as:

$$C_{ijkl}^H = \frac{1}{|Y|} \int_Y \left(C_{ijkl} - C_{ijpq} \frac{\partial \chi_p^{kl}}{\partial y_q} \right) dY \tag{18}$$

Fig. 10 Comparison between the stiffness of hexagonal element patterns, checkerboard pattern, and homogeneous distribution of material (SIMP with $p = 3$ is used unless otherwise noted)



where C_{ijkl} are elastic stiffness coefficients at a given point in the unit cell; C_{ijkl}^H are homogenized stiffness coefficients; Y is the periodic domain, which is the area of the unit cell shown in Fig. 9; and χ_p^{kl} are characteristic displacements obtained by solving the following equation:

$$\int_Y C_{ijpq} \frac{\partial \chi_p^{kl}}{\partial y_q} \frac{\partial v_i}{\partial y_j} dY = \int_Y C_{ijkl} \frac{\partial v_i}{\partial y_j} dY, \forall v \in V_h \tag{19}$$

Here V_h is the set of all Y -periodic functions.

Using finite element discretization, one obtains the characteristic displacement by solving the following equation:

$$\mathbf{K} \chi^{(kl)} = \mathbf{f}^{(kl)} \tag{20}$$

where \mathbf{K} is the standard stiffness matrix; and $\mathbf{f}^{(kl)}$ is the material load corresponding to test strain kl , calculated from:

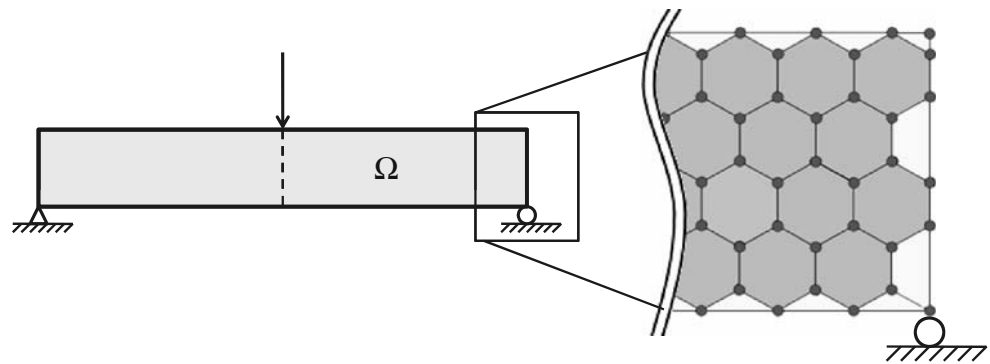
$$\mathbf{f}^{(kl)} = \sum_e \int_{\Omega_e} \mathbf{B}_e^T \mathbf{C}_e(y) \boldsymbol{\varepsilon}^{0(kl)} dy \tag{21}$$

In this expression, \mathbf{B}_e is the standard kinematic matrix; \mathbf{C}_e is the constitutive matrix, and $\boldsymbol{\varepsilon}^{0(kl)}$ is the test strain. The homogenized stiffness tensor is given by:

$$C_{ijkl}^H = \frac{1}{|Y|} \sum_e (\chi^{0(ij)} - \chi^{(ij)}) \mathbf{K}_e (\chi^{0(kl)} - \chi^{(kl)}) \tag{22}$$

It is worth noting that for the imposition of periodic boundary conditions, we have used regular node numbering along with multipoint constraints (e.g., Cook et al. 2002). This is different from the traditional treatment of periodicity that involves the use of repeated node numbers. Such an approach in the context of

Fig. 11 Schematic representation of the design domain, loading and boundary conditions for MBB (Messerschmitt-Bölkow-Blohm) beam problem. Notice that the non-hexagonal elements on the boundary are either triangles or quads



homogenization with polygonal cells is discussed by Diaz and Benard (2003).

We study four arbitrary small scale patterns of hexagonal mesh, which may appear in topology optimization results. These patterns are those with potentially high stiffness and are shown in Fig. 9. The results of this investigation are illustrated in Fig. 10 where the stiffness of hexagonal patterns along with the checkerboard of Q4 elements and homogenous material distribution are plotted. Also included in the plot is the stiffness of the homogenous material distribution subjected to no penalization. In all other cases, the penalization parameter is taken as 3.

For each pattern, the density of “black” elements is increased from 0 to 1. The horizontal axis shows the *total* volume fraction of the pattern. Note that each plot ends at the point corresponding to the configuration shown in Fig. 9 with black elements having density of one. Therefore, the checkerboard plot terminates at volume fraction 0.5 while the plot for pattern 1 ends at volume fraction of $2/3$ (this pattern has 4 black elements and 2 white elements in its unit cell). Only the result of C_{1111}^H is calculated. Other stiffness coefficients can be computed in a similar manner.

As shown in Fig. 10, the black–white checkerboard pattern avoids penalization: the black–white checkerboard (volume fraction 0.5), modeled by Q4 elements, has stiffness equal to the homogenous distribution with no penalization ($p = 1$). This is in agreement with the results presented by Diaz and Sigmund (1995). The patterns of hexagonal elements, however, are not as overly stiff as the checkerboard pattern because their stiffness curves lie below the line of no penalization. Moreover, the homogenized stiffness of the hexagonal patterns is closer to the stiffness of penalized homogeneous distribution (obtained using SIMP with $p = 3$). These results demonstrate that the formation of undesired small scale patterns in the results of topology optimization is alleviated when using Wachspress hexagonal elements. As we shall see in the next section, the topology optimization results obtained with the Wachspress elements confirm this conclusion.

8 Numerical results

The benchmark MBB-beam problem (see, for example, Olhoff et al. 1991) is solved using the Wachspress hexagonal element and results are compared with the

Fig. 12 MBB beam design with element-based formulation: **a–c** results with Q4 elements and **d–f** results with H6/U (hexagonal) elements. Boundary elements were added to achieve domain closure. The mesh discretization is 60×20 , 90×30 , 120×40 from *top to bottom*, respectively, for both implementations

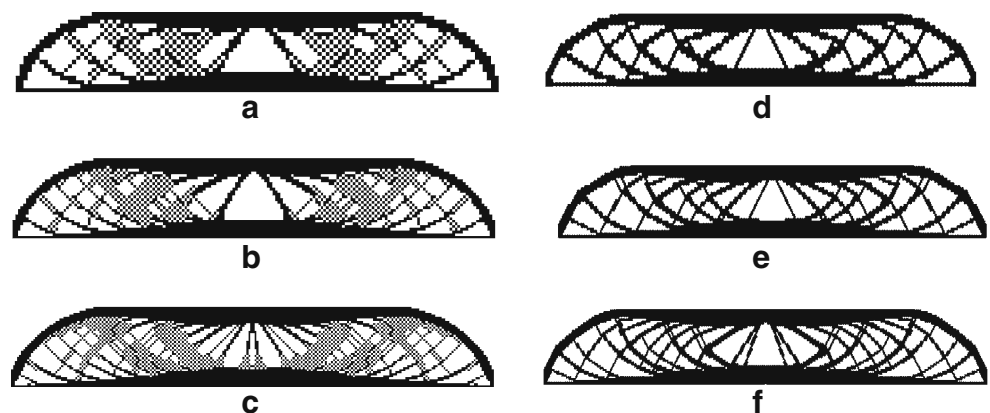
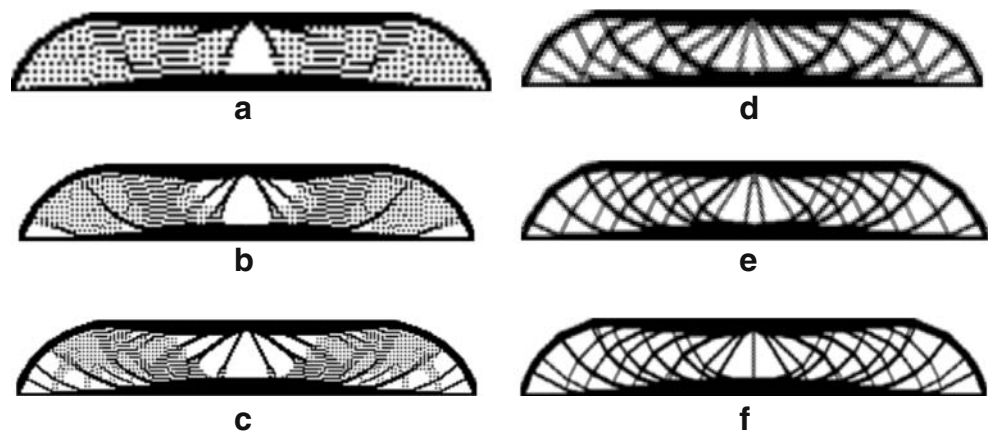


Fig. 13 MBB beam design with CAMD approach: **a–c** results with Q4/Q4 elements and **d–f** results with H6/H6 (hexagonal) elements. Boundary elements were added to achieve domain closure. The mesh discretization is 60×20 , 90×30 , 120×40 from *top to bottom*, respectively for both implementations



corresponding Q4 implementation. Due to the symmetry of the problem, only half of the MBB-beam is considered (Fig. 11). The beam has an aspect ratio of 6:1, and three levels of mesh discretization are used. The Poisson's ratio of the material is taken to be 0.3, while V_s is 50% of volume of the design domain. We solved the minimum compliance problem using the Method of Moving Asymptotes (MMA) developed by Svanberg (1987). In addition, we used a continuation method on the value of p to avoid converging to local minima. The value of p was gradually increased (using increments of 0.5) from 1 to 4 after sufficient convergence for each value of p . The optimization results for the element-based and projection schemes are plotted using the element densities ρ_e . For the CAMD results, the continuous density $\rho(\mathbf{x})$ is shown in an average sense: the average of ρ_e^c is obtained and plotted for each hexagonal element.

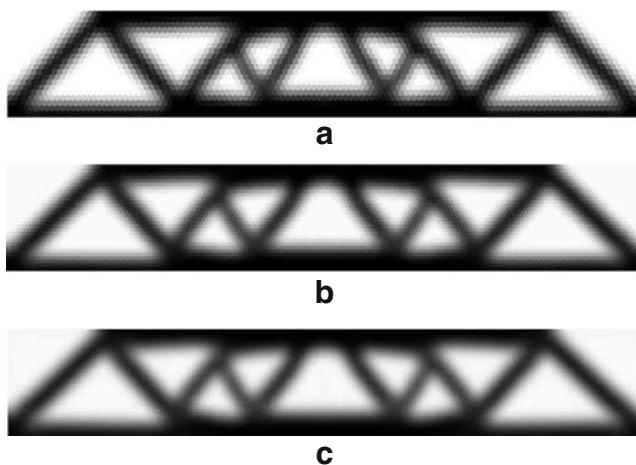


Fig. 14 MBB beam design with projection approach ($r_{\min} = 0.15h$ where h is the height of the beam): **a–c** results with hexagonal elements. The mesh discretization is 60×20 , 90×30 , 120×40 from *top to bottom*, respectively

In Fig. 12, the results of the element-based formulation for the Q4 element and the hexagonal element for various levels of mesh refinement are shown. The solutions with Q4 implementation contain patches of checkerboard while no such fine scale patterns are observed with the Wachspress implementation. Note that no filtering technique or density gradient was imposed and thus the checkerboard-free property of the hexagonal element is attributed essentially to its geometric features and interpolation characteristics.

Figure 13 shows the results of CAMD approach for the MBB-beam design for both Q4 and Wachspress implementation. Note that in this case, the density and displacement fields are interpolated using the same shape functions for each element discretization. We can observe that the Q4/Q4 results suffer from spurious islanding and layering patterns, which is in agreement with the findings of Rahmatalla and Swan (2004). The designs using Wachspress elements, however, show no signs of such instability. Therefore, the Wachspress element performance in this case is attributed to its interpolation characteristics. We note that our numerical results for the MBB-beam agree closely with the exact analytical solutions derived by Lewinski et al. (1994).

Finally, the results using projection scheme are presented in Fig. 14. The radius of the projection r_{\min} is taken to be 0.15 of the height of the beam and independent of the mesh size. We can see that despite the change in the level of mesh refinement, the same design is obtained in all cases. The length scale imposed on the optimization through r_{\min} guarantees mesh-independent solutions that satisfy the required minimum member size.

9 Concluding remarks

In this work, the checkerboard pathology in topology optimization is addressed and circumvented by means

of a new finite element. The proposed hexagonal element with Wachspress-type shape functions is shown to possess advantages over conventional finite elements. Geometric properties of the hexagonal element, such as two-node connections and symmetry in three edge-based directions, are among its distinguishing features. As discussed and demonstrated by examples, the use of hexagonal elements eliminates the formation of checkerboard and other numerical anomalies, and provides a robust and stable means for solving topology optimization problems.

The present approach may be extended to three-dimensional topology optimization by noting the features employed to eliminate the checkerboard and other instabilities. Such extension requires: (i) a mesh that excludes point and edge contact, i.e., a mesh in which two connected elements share a face; and (ii) selection of an appropriate finite element interpolation or enrichment scheme.

A few remarks regarding the use of honeycomb finite elements are in order. Reliance on a particular finite element formulation may naturally impose limitations from practical perspective. Such objection can also be made to the use of nonconforming or higher order elements. Indeed there is a trade-off: conventional elements like quads and triangles are widely used but suffer from serious instabilities unless additional constraints are imposed. The implementation of these constraints is not always straightforward or desirable. On the other hand, particular formulations, such as the one presented in this paper, may be better suited for topology optimization, even though they are less commonly used. Moreover, there have been several recent papers in the literature (see review paper by Sukumar and

Malsch 2005) that address polygonal finite elements. As these elements become more popular and widespread, solutions such as the one contributed by our work have the potential to become more popular and practical.

The honeycomb element together with the topology optimization formulation has promising extensions, such as design of microelectromechanical systems and piezoelectric actuators (Carbonari et al. 2007a, b; Sigmund 2001). Future investigations include the use of higher-order Wachspress elements (see, for example, Gout 1985). In addition, the CAMD approach may be investigated for meshes in which the displacement and density locations are not coincident in the element, which would allow for a more flexible density field discretization. Furthermore, nonlinear weight functions can be studied in conjunction with the projection method (see Section 6.3). Such considerations have the potential to lead to enhanced Wachspress elements for high-fidelity topology optimization.

Acknowledgements We acknowledge the support by the Department of Energy Computational Science Graduate Fellowship Program of the Office of Science and National Nuclear Security Administration in the Department of Energy under contract DE-FG02-97ER25308. We are grateful to Prof. Krister Svanberg for providing his MMA (Method of Moving Asymptotes) code, which was used to generate the examples in this paper. We acknowledge the anonymous reviewer for pointing out the references by Saxena and Saxena (2007) and Langelaar (2007). Finally, we thank Dr. Ivan F. M. Menezes for insightful discussions and suggestions.

Appendix

Quadrature rule for Wachspress hexagonal element (from Lyness and Monegato 1977): Table 1

Table 1 Quadrature parameters as defined in Section 5

<i>N</i>	<i>j</i>	α_j	r_j	w_j
1	0	0.0000000000000000	0.0000000000000000	0.255952380952381
	1	0.0000000000000000	0.748331477354788	0.124007936507936
2	0	0.0000000000000000	0.0000000000000000	0.174588684325077
	1	0.0000000000000000	0.657671808727194	0.115855303626943
	2	0.523681372148045	0.943650632725263	0.021713248985544
3	0	0.0000000000000000	0.0000000000000000	0.110826547228661
	1	0.0000000000000000	0.792824967172091	0.037749166510143
	2	0.523598775598299	0.537790663359878	0.082419705350590
	3	0.523598775598299	0.883544457934942	0.028026703601157
4	0	0.0000000000000000	0.0000000000000000	0.087005549094808
	1	0.0000000000000000	0.487786213872069	0.071957468118574
	2	0.0000000000000000	0.820741657108524	0.027500185650866
	3	0.523598775598299	0.771806696813652	0.045248932131663
	4	0.523598775598299	0.957912268790000	0.007459892497607

References

- Ambrosio L, Buttazzo G (1993) An optimal design problem using perimeter penalization. *Calc Var Partial Differ Equ* 1:55–69
- Bendsøe MP (1989) Optimal shape design as a material distribution problem. *Struct Optim* 1:193–202
- Bendsøe MP, Kikuchi N (1988) Generating optimal topology in structural design using a homogenization method. *Comput Methods Appl Mech Eng* 71:197–224
- Bendsøe MP, Sigmund O (1999) Material interpolation schemes in topology optimization. *Arch Appl Mech* 69:635–654
- Bendsøe MP, Sigmund O (2003) *Topology optimization-theory, methods and applications*. Springer Verlag, New York
- Borrvall T, Petersson J (2001a) Large-scale topology optimization in 3D using parallel computing. *Comput Methods Appl Mech Eng* 190(46–47):6201–6229
- Borrvall T, Petersson J (2001b) Topology optimization using regularized intermediate density control. *Comput Methods Appl Mech Eng* 190:4911–4928
- Bruns TE (2005) A re-evaluation of the SIMP method with filtering and an alternative formulation for solid-void topology optimization. *Struct Multidisc Optim* 30:428–436
- Carbonari RC, Silva ECN, Paulino GH (2007a) Multi-actuated functionally graded piezoelectric micro-tools design: a multi-physics topology optimization approach. *Int J Numer Methods Eng* (in press)
- Carbonari RC, Silva ECN, Paulino GH (2007b) Topology optimization design of functionally graded bimorph-type piezoelectric actuators. *Smart Mater Struct* 16(6):2605–2620
- Chavey D (1989) Tilings by regular polygons 2. A catalog of Tilings. *Comput Math Appl* 17(1–3):147–165
- Cook RD, Malkus DS, Plesha ME (2002) *Concepts and applications of finite element analysis*, 4th. edn. Wiley, New York
- Costa JCA, Alves MK (2003) Layout optimization with h-adaptivity of structures. *Int J Numer Methods Eng* 58(1): 83–102
- Dalton GR (1985) Automatic indexed calculation of Wachspress' rational finite element functions. *Comput Math Appl* 11(6):621–623
- Dasgupta G (2003) Interpolants within convex polygons: Wachspress' shape functions. *J Aerosp Eng* 16(1):1–8
- Diaz A, Benard A (2003) Designing materials with prescribed elastic properties using polygonal cells. *Int J Numer Methods Eng* 57(3):301–314
- Diaz A, Sigmund O (1995) Checkerboard patterns in layout optimization. *Struct Optim* 10:40–45
- Gout JL (1985) Rational Wachspress-type finite elements on regular hexagons. *IMA J Numer Anal* 5(1):59–77
- Guest J, Prevost J, Belytschko T (2004) Achieving minimum length scale in topology optimization using nodal design variables and projection functions. *Int J Numer Methods Eng* 61(2):238–254
- Haber RB, Jog CS, Bendsøe MP (1996) A new approach to variable-topology shape design using a constraint on perimeter. *Struct Optim* 11:1–12
- Jang G, Jeong H, Kim Y, Sheen D, Park C, Kim M (2003) Checkerboard-free topology optimization using non-conforming finite elements. *Int J Numer Methods Eng* 57: 1717–1735
- Jang G, Lee S, Kim Y, Sheen D (2005) Topology optimization using non-conforming finite elements: three-dimensional case. *Int J Numer Methods Eng* 63:859–875.
- Jog CS, Haber RB (1996) Stability of finite element models for distributed-parameter optimization and topology design. *Comput Methods Appl Mech Eng* 130:203–226
- Kim J, Paulino GH (2002) Isoparametric graded finite elements for nonhomogeneous isotropic and orthotropic materials. *J Appl Mech Trans ASME* 69(4):502–514
- Kohn RV, Strang G (1986) Optimal design and relaxation of variational problems. *Commun Pure Appl Math* 39, Part I: 1–25, Part II: 139–182, Part III: 353–377
- Lewinski T, Zhou M, Rozvany GIN (1994) Extended exact least-weight truss layouts—part II: unsymmetric cantilevers. *Int J Mech Sci* 36:399–419
- Lyness JN, Monegato G (1977) Quadrature rules for regions having regular hexagonal symmetry. *SIAM J Numer Anal* 14(2):283–295
- Matsui K, Terada K (2004) Continuous approximation of material distribution for topology optimization. *Int J Numer Methods Eng* 59:1925–1944
- Maute K, Ramm E (1995) Adaptive topology optimization. *Struct Optim* 10:100–112
- Murat F, Tartar L (1985) Optimality conditions and homogenization. *Proceedings of Nonlinear variational problems (Isola d'Elba, 1983)*, Res. Notes in Math., vol 127. Pitman, Boston, pp 1–8
- Olhoff N, Bendsøe MP, Rasmussen J (1991) On CAD-integrated structural topology and design optimization. *Comput Methods Appl Mech Eng* 89:259–279
- Paulino GH, Silva ECN (2005) Design of functionally graded structures using topology optimization. *Materials Science Forum*, 492–493, 435–440. Trans Tech Publications, Switzerland
- Petersson J, Sigmund O (1998) Slope constrained topology optimization. *Int J Numer Methods Eng* 41(8):1417–1434
- Pomezanski V, Querin OM, Rozvany GIN (2005) CO-SIMP: extended SIMP algorithm with direct Corner Contact Control. *Struct Multidisc Optim* 30:164–168
- Poulsen TA (2002a) A simple scheme to prevent checkerboard patterns and one-node connected hinges in topology optimization. *Struct Multidisc Optim* 24:396–399
- Poulsen TA (2002b) Topology optimization in wavelet space. *Int J Numer Methods Eng* 53:567–582
- Poulsen TA (2003) A new scheme for imposing minimum length scale in topology optimization. *Int J Numer Methods Eng* 57(6):741–760
- Langelaar M (2007) The use of convex uniform honeycomb tessellations in structural topology optimization. *Proceedings of the 7th world congress on structural and multidisciplinary optimization*, Seoul, South Korea, 21–25 May 2007
- Rahmatalla SF, Swan CC (2004) A Q4/Q4 continuum structural topology optimization. *Struct Multidisc Optim* 27:130–135
- Saxena R, Saxena A (2007) On honeycomb representation and SIGMOID material assignment in optimal topology synthesis of compliant mechanisms. *Finite Elem Anal Des* 43: 1082–1098
- Sigmund O (2001) Design of multiphysics actuators using topology optimization—part II: two-material structures. *Comput Methods Applied Mech Eng* 190(49–50):6605–6627
- Sigmund O (2007) Morphology-based black and white filters for topology optimization. *Struct Multidisc Optim* 33:401–424
- Sigmund O, Petersson J (1998) Numerical instabilities in topology optimization: a survey on procedures dealing with checkerboard, mesh-dependence and local minima. *Struct Optim* 16:68–75

- Silva E, Carbonari R, Paulino GH (2007) On graded elements for multiphysics applications. *Smart Mater Struct* 16:2408–2428
- Sukumar N, Malsch EA (2005) Recent advances in the construction of polygonal finite element interpolants. *Arch Comput Methods Eng* 11:1–38
- Sukumar N, Tabarraei A (2004) Conforming polygonal finite elements. *Int J Numer Methods Eng* 61:2045–2066
- Svanberg K (1987) The method of moving asymptotes—a new method for structural optimization. *Int J Numer Methods Eng* 24:359–373
- Talischi C, Paulino GH, Le CH (2008) Topology optimization using Wachspress-type interpolation with hexagonal elements. In: Paulino GH et al (ed) *Multiscale and functionally graded materials 2006 (M&FGM 2006)*, AIP conference proceedings, vol 973. American Institute of Physics, Melville, New York, pp 309–316
- Wachspress EL (1975) *A rational finite element basis*. Academic Press, New York
- Wang S (2007) *Krylov subspace methods for topology optimization on adaptive meshes*. PhD dissertation, University of Illinois at Urbana-Champaign, Urbana, Illinois, USA.
- Wang M, Wang S (2005) Bilateral filtering for structural topology optimization. *Int J Numer Methods Eng* 63:1911–1938
- Warren J (2003) On the uniqueness of barycentric coordinates. *Contemporary mathematics: proceedings of AGGM'02*, pp 93–99
- Yoon GH, Kim YY (2005) Triangular checkerboard control using a wavelet-based method in topology optimization. *Int J Numer Methods Eng* 63:103–121
- Zhou M, Rozvany GIN (1991) The COC algorithm, part II: topological, geometry and generalized shape optimization. *Comput Methods Appl Mech Eng* 89:197–224